Finite element investigations for the construction of composite solutions of even-parity transport equation

Anwar M. Mirza and Shaukat Iqbal

Abstract. Finite element investigations have been carried out to construct composite solutions of transport problems. A variational principle K_λ^+ has been implemented numerically, which admitted the use of discontinuous trial functions at the interfaces of regions. The spatial variations of the angular flux have been modeled by finite elements, while Legendre polynomials have been utilized to represent the directional dependence. A computer code has been written for one group multi-regions problems in one dimension. Different orders of angular approximations have been employed for the angular flux to reduce computing time. The composite solutions are compared with the exact solutions as well as with the conventional continuous finite elements solutions.

M.S.C. 2000: 80M10, 82D75, 80M30, 35R05.
Key words: Finite element method, Boltzmann transport equation, variational principles, discontinuous formulation.

§1. Introduction

Neutron transport problems have been solved in various different ways by using finite element method ([3], [4], [11], [14]). A weighted residuals approach is adopted in some formulations, while in others, variational approaches are considered. Euler-Lagrange, bi-linear functionals and generalized least squares methods are variational methods. The generalized least-squares method for neutron transport problems was given by Ackroyd [3]. Already established and new extremum principles can be generated by this method for both steady state and time dependent transport problems. This method was also used to generate variational principles for both first and second order forms of neutron transport equation [1].

The exact solution of the neutron transport equation for angular flux is a continuous function of position and direction variables. However, in many practical situations steep or even abrupt changes in the angular flux can be encountered. For example, at a point on the interface of different media, the angular flux is not continuous for directions lying in the tangential plane to the interface. In a strongly heterogeneous medium, Martin and Duderstadt [8] have shown that substantial discontinuities exist at for various interfaces. The gradient of flux may be very steep at certain interfaces,

Applied Sciences, Vol.9, 2007, pp. 121-140.

e.g. at an interface between a source and a strong absorber. Such abrupt changes may better be predicted with the help of discontinuous finite elements. Another advantage of the use of discontinuous finite elements is that different orders of angular approximations may be used on the two sides of an interface. In such cases diffusion theory can be applied in those regions where transport effects are not prominent, while transport calculations can be performed with finer elements meshes in particular regions. Wilson [14] used discontinuous finite elements in principle, which employs both even and odd parity fluxes. A maximum principle has been developed by Ackroyd [2] which admits both continuous and discontinuous finite elements for the even parity form of the neutron transport equation. This principle not only ensures a global particle balance for the whole domain, but also gives a detailed balance on region by region scale if used in conjunction with a discontinuous approach. It employs a penalty parameter to control the jumps in the angular flux at element interfaces. In this paper principle is used to obtain composite solutions for neutron transport problems with the help of discontinuous finite elements. Lagrange interpolation functions have been used as spatial trial functions and Legendre polynomials for angular representation.

§2. Theoretical background

The neutron transport process is governed by a first order integro-differential equation called Boltzmann Transport Equation. The distinguishing features of the transport process are the large mean free paths and less frequent collisions compared to small mean free paths and more frequent collisions of the particles in the diffusion process.

2.1 Second Order Even-Parity Transport Equations

The first order neutron transport equation in its steady state one energy group form can be written as:

$$\Omega \cdot \nabla\phi + \sigma(r)\phi(r,\Omega) = \int_{4\pi} d\Omega' \sigma_s(r,\Omega' \to \Omega)\phi(r,\Omega') + s(r,\Omega) \tag{2.1}$$

where $\phi(r,\Omega)$ is the angular flux, $\sigma(r)$ is the total macroscopic cross-section, $\sigma_s(r,\Omega' \to \Omega)$is the differential form of the macroscopic scattering cross-section and $s(r,\Omega)$ is the rate of production of source neutrons.
In most practical applications, the scattering collisions have got rotational symmetry, i.e. the scattering cross-section is independent of the incident and scattered directions, but depends upon the cosine of the angle between the two directions. Thus:

$$\sigma_s(r,\Omega' \to \Omega) = \sigma_s(r,\Omega' \cdot \Omega) = \sigma_s(r,\mu_0) \tag{2.2}$$

Therefore, the scattering kernel can be expanded in terms of Legendre polynomial as:

$$\sigma_s(r,\mu_0) = \sum_{l=0}^{\infty} \left(\frac{2l+1}{4\pi}\right) \sigma_{sl}(r) P_l(\mu_0) \tag{2.3}$$

where $P_l(\mu_0)$ is the Legendre polynomial of order l and the scattering coefficient σ_{sl} is given by the orthogonality of Legendre Polynomials as:

$$\sigma_{sl} = 2\pi \int_{-1}^{+1} d\mu_0 \sigma_s(r, \mu_0) P_l(\mu_0) \tag{2.4}$$

Thus within group steady-state neutron transport equation can be written as,

$$\Omega \cdot \nabla\phi(r,\Omega) + \sum_{l=0}^{\infty} \left(\frac{2l+1}{4\pi}\right) \sigma_l(r) \int_{4\pi} d\Omega' \phi(r,\Omega') P_l(\Omega' \cdot \Omega) = s(r,\Omega) \tag{2.5}$$

where

$$\sigma_l(r) = \sigma(r) - \sigma_{sl}(r) \tag{2.6}$$

The second order forms of the transport equation are obtained by splitting the angular flux $\phi(r,\Omega)$ into even- $\psi(r,\Omega)$ and odd-parity $\chi(r,\Omega)$ components, defined by:

$$\begin{array}{rcl} \psi(r,\Omega) & = & \frac{1}{2}\left[\phi(r,\Omega) + \phi(r,-\Omega)\right] \\ \chi(r,\Omega) & = & \frac{1}{2}\left[\chi(r,\Omega) - \chi(r,-\Omega)\right] \end{array} \tag{2.7}$$

and the even- and odd-parity sources are defined as:

$$s^{\pm}(r,\Omega) = \frac{1}{2}\left[s(r,\Omega) \pm s(r,-\Omega)\right] \tag{2.8}$$

These parity fluxes and sources are substituted into the first order transport equation to obtain the mixed parity equations:

$$\begin{array}{rcl} \Omega \cdot \nabla\chi(r,\Omega) + H\psi(r,\Omega) & = & s^{+}(r,\Omega) \\ \Omega \cdot \nabla\psi(r,\Omega) + G^{-1}\chi(r,\Omega) & = & s^{-}(r,\Omega) \end{array} \tag{2.9}$$

where the leakage G and removal H operators are defined as:

$$\begin{array}{rcl} Gf(r,\Omega) & = & \sum_{lodd} \left(\frac{2l+1}{4\pi}\right) \sigma_l^{-1}(r) \int_{4\pi} d\Omega' f(r,\Omega') P_l(\Omega' \cdot \Omega) \\ Hf(r,\Omega) & = & \sum_{leven} \left(\frac{2l+1}{4\pi}\right) \sigma_l(r) \int_{4\pi} d\Omega' f(r,\Omega') P_l(\Omega' \cdot \Omega) \end{array} \tag{2.10}$$

Both the operators G and H and their inverse G^{-1} and H^{-1} are both self-adjoint and positive definite. Second order equations for the even-parity flux $\psi(r,\Omega)$ can be obtained from the (2.9) and are given by:

$$-\Omega \cdot \nabla G[\Omega \cdot \nabla \psi] + H\psi(r,\Omega) = s^{+}(r,\Omega) - \Omega \cdot \nabla G[s^{-}(r,\Omega)] \tag{2.11}$$

This equation is called even-parity transport equation. This parity flux is in general subjected to bare surface, perfect reflector, surface with source and interface surface type boundary conditions. These conditions along with their illustrations are listed in Table (1).

Table 1: Boundary Conditions for the Even-Parity Transport Equation

Surface Type	Boundary Condition
Bare Surface[a] S_b	$\psi_0 + G\left[s^{-} - \Omega \cdot \nabla \psi_0\right] = 0$ for $\Omega \cdot n < 0$ $\psi_0 - G\left[s^{-} - \Omega \cdot \nabla \psi_0\right] = 0$ for $\Omega \cdot n > 0$
Surface S_s with source $T(r,\Omega)$	$\psi_0 + G\left[s^{-} - \Omega \cdot \nabla \psi_0\right] = T(r,\Omega)$ for $\Omega \cdot n < 0$ $\psi_0 - G\left[s^{-} - \Omega \cdot \nabla \psi_0\right] = T(r,\Omega)$ for $\Omega \cdot n > 0$
Perfect Reflector[b] S_{pr}	$\psi_0(r,\Omega) = \psi_0(r,\Omega^{*})$ $G\left[s^{-}(r,\Omega) - \Omega \cdot \nabla \psi_0(r,\Omega) - s^{-}(r,\Omega^{*}) + \Omega^{*} \cdot \nabla \psi_0(r,\Omega^{*})\right] = 0$
Inreface Surface[c] $S_i \cap S_j$	$\psi_0(r,\Omega)$ and $G\left[s^{-} - \Omega \cdot \nabla \psi_0\right]$ are continuous for $\Omega \cdot n_i \neq 0$

[a] n is an outward normal to the exterior surface
[b] Ω^{*} is the reflected direction to the incident direction Ω
[c] n_i is the outward normal to the surface S_i

2.2 $K^{+}[\psi]$, a variational principle admitting continuous trial functions

$K^{+}[\psi]$ principle is a maximum principle for solving even parity neutron transport equation. This principle admits trial functions which are continuous in space and angular variables. The variational functional $K^{+}[\psi]$ can be written as:

$$K^{+}[\psi] = 2F_s^{+}[\psi] - F^{+}[\psi,\psi] \tag{2.12}$$

In particular, for one dimensional slab geometry, with a surface source $T(r,\Omega)$ and with an isotropic fixed source, the functionals $F^{+}[\psi_1,\psi_2]$ and $F_s^{+}[\psi_1]$ can be written as:

$$\begin{aligned} F^{+}\left[\psi_1,\psi_2\right] &= 2\pi \int_a^b dx \int_{-1}^{+1} d\mu \left[\mu \frac{\partial \psi_1}{\partial x} G\mu \frac{\partial \psi_2}{\partial x} + \psi_1 H \psi_2\right] \\ &+ 2\pi \int_{-1}^{+1} d\mu\, |\mu| \left[l_a \psi_1(a,\mu)\psi_2(a,\mu) + l_b \psi_1(b,\mu)\psi_2(b,\mu)\right] \\ &+ 2\pi \int_{-1}^{+1} d\mu\, |\mu| \left[k_a \psi_1(a,\mu)\psi_2(a,\mu) + k_b \psi_1(b,\mu)\psi_2(b,\mu)\right] \end{aligned} \tag{2.13}$$

$$
\begin{aligned}
F_s^+[\psi_1] &= 2\pi \int_{x=a}^{b} dx \int_{-1}^{+1} d\mu \left[\psi_1 s^+ + \mu \tfrac{\partial \psi_1}{\partial x} G s^-\right] \\
&+ 4\pi \int_{-1}^{+1} d\mu\, |\mu| \left[k_a \psi_1(a,\mu) T(a,\mu) + k_b \psi_1(b,\mu) T(b,\mu)\right]
\end{aligned} \tag{2.14}
$$

where $(b-a)$ is the thickness of the slab. Also $l_a = 0$ for a perfect reflector S_{pr} and $l_a = 1$ for a bare surface, and vice versa. Also $k_a = 0$ for surface without source and $k_a = 1$ for a surface with a source.

2.3 $K_\lambda^+[\psi]$, a variational principle admitting continuous trial functions

The $K_\lambda^+[\psi]$ functional admits trial functions which are in general discontinuous across the interfaces of the elements. Maximum principle is written as:

$$
\begin{aligned}
K_\lambda^+[\psi] &= K^+[\psi] \\
&- \left\{ \begin{array}{l} \lambda^+ \int\limits_{\cup(S_i \cap S_j)} \int\limits_{4\pi} \{\Omega \cdot n_i [\psi(r_i,\Omega) - \psi(r_j,\Omega)]\} \\ G\{\Omega \cdot n_i [\psi(r_i,\Omega) - \psi(r_j,\Omega)]\}\, d\Omega dS \end{array} \right\} \\
&\leq F^+[\psi_0,\psi_0] + \tfrac{1}{\lambda^+} \int\limits_{\cup(S_i \cap S_j)} dS \int\limits_{4\pi} d\Omega \chi_0 G^{-1} \chi_0
\end{aligned} \tag{2.15}
$$

where λ^+ is a positive number called penalty parameter, and is used to control the jump discontinuity $[\psi(r_i,\Omega) - \psi(r_j,\Omega)]$ at an interface $S_i \cap S_j$. The proof and derivation of the $K_\lambda^+[\psi]$ maximum principle is given elsewhere [7][8]. For the particular case of one dimensional slab geometry, this principle can be written as:

(2.16)

$$
\begin{aligned}
K_\lambda^+[\psi] &= K^+[\psi] \\
&- \lambda^+ \textstyle\sum_{i=1}^{N_f} \displaystyle\int_{-1}^{+1} d\mu \{\mu [\psi(x_i,\mu) - \psi(x_j,\mu)]\} G\{\mu [\psi(x_i,\mu) - \psi(x_j,\mu)]\}
\end{aligned}
$$

where N_f is the number of interfaces.

§3. The finite element formulation

3.1 Finite element trial functions for even-parity angular flux

The spatial domain is first of all discretized into a finite number of sub-domains called finite elements. The spatial dependence of the even-parity angular flux is represented in terms of the nodal values of the flux and the finite element shape functions. Also even order Legendre polynomials have been used to represent the directional dependence of the even-parity flux respectively. This representation is

equivalent to an odd P_N method [9]. The even parity flux can thus be approximated by the trial functions $\psi(x, \mu)$ as:

$$\psi(x, \mu) = B^T(x) \otimes Q^T(\mu)\underline{\psi} \tag{3.17}$$

3.2 Finite element trial functions for spatial domain

The spatial domain is discretized into E elements. Each element has N_e nodes (which can vary from region to region). The angular moments $\psi_l(x)$ for even-parity are then expanded in terms of a linear combination of spatial basis $B_i^e(x)$ for element$e$ and the nodal values. Thus the even-parity angular moments $\psi_l(x)$ can be written for an element e as:

$$\psi_l^e(x) = B^{eT}(x)\underline{\psi}_l^e \tag{3.18}$$

Element shape functions $B_i(x)$ can be represented in various different ways. In case of Lagrange polynomial interpolation, the shape function $B_i(x)$ can be written as

$$B_i^e(x) = \prod_{k=1, k\neq i}^{N_e} \frac{(x - x_k)}{(x_i - x_k)} \tag{3.19}$$

3.3 The discretized K^+ functional

The maximum principle given by K^+ functional admits continuous trial functions. The trial functions are forced to obey the continuity condition at the interfaces between the regions. Substitution of the even parity trial function from (3.17) into K^+ functional (2.12) gives us the discretized K^+ functional:

$$K^+[\psi] = \sum_{e=1}^{E} K^{+e}(\psi) = \sum_{e=1}^{E} \{2F_s^{+e}[\psi] - F^{+e}[\psi, \psi]\} \tag{3.20}$$

and later maximization of the local functional $K^{+e}[\psi]$ with respect to the unknown coefficient $\underline{\psi}^e$ vector gives the following local set of simultaneous linear algebraic equations:

$$A^e\underline{\psi}^e = B^e \tag{3.21}$$

where A^e is the element stiffness matrix and B^e is the element source vector. A^e is a symmetric matrix. For all the elements apart from the boundary elements, its general form is given by:

$$A^e = S_3^e \otimes A_3 + S_2^e \otimes A_2 \tag{3.22}$$

while for the boundary elements it can be written as:

$$A^e = S_3^e \otimes A_3 + S_2^e \otimes A_2 + l_i S_4^e \otimes A_4 + k_i S_4^e \otimes A_4 \tag{3.23}$$

where $l_i = 0$ for a perfect reflector and $l_i = 1$ for a bare surface. $k_i = 0$ for surface without source and $k_i = 1$ for surface with a source. Also the element source vector can be written as,

$$B^e = S_1^e \otimes A_1 + k_i S_1^i \otimes A_1^i \tag{3.24}$$

The S_i^e matrices contain all spatial integrations and are dependent only on the type of the element being used. Similarly, all angular integrations are grouped in A_i matrices, which depend on the material properties and the order of angular approximation being used. The definitions of both spatial and angular matrices are given in Table (2).

Table 2: Angular and Spatial Matrices

Matrix	Definition
A_1	$\int_{-1}^{+1} s^+(x,\mu)Q(\mu)d\mu$
A_2	$\sum_{leven}^{N-1} \left(\frac{2l+1}{2}\right) \sigma_l \int_{-1}^{+1} P_l(\mu)Q(\mu)d\mu \int_{-1}^{+1} P_l(\mu)Q^T(\mu)d\mu$
A_3	$\sum_{lodd}^{N} \left(\frac{2l+1}{2}\right) \sigma_l^{-1} \int_{-1}^{+1} P_l(\mu)Q(\mu)d\mu \int_{-1}^{+1} P_l(\mu)Q^T(\mu)d\mu$
A_4	$2\int_{0}^{+1} \mu Q(\mu)Q^T(\mu)d\mu$
S_1^e	$\int_{x_1}^{x_2} B^e(x)dx$
S_2^e	$\int_{x_1}^{x_2} B^e(x)B^{eT}(x)dx$
S_3^e	$\int_{x_1}^{x_2} \frac{dB^e}{dx}\frac{dB^{eT}}{dx}dx$
S_4^e	$B^e(x_i)B^{eT}(x_i)dx$, x_i is the boundary node

Following the general finite element modeling technique, all the local systems of equations are assembled to form the global set of algebraic equations:

$$A\underline{\psi} = B \tag{3.25}$$

where A is the global stiffness matrix and the B is the global source vector. In this case the global system is obtained by forcing the continuity of the trial function

at element interfaces and making use of element connectivity. The global matrix A is a diagonally dominant, symmetric and banded matrix. The symmetric and diagonally dominant properties of the global matrix are due to the self-adjoint and positive definite nature respectively of the operator G and H used in the even parity formulation of the problem. These features ensure the stability and convergence of the solution. A banded system is obtained because each element in the finite element grid is connected to only to its neighbouring elements. Because of the banded and symmetric nature of the global matrix, only the upper half band of the matrix is needed to be stored, thus reducing the computer storage requirements.

3.4 The discretized K_λ^+ functional

K_λ^+ functional admits not only the continuous but also discontinuous trial functions. The discontinuous trial functions do not have to obey the continuity condition at the region interfaces. In the work presented, discontinuities are considered at all interfaces between adjoining regions.
These types of discontinuities at adjoining interfaces have the advantage that different orders of angular approximations can be considered in different regions. In one dimensional slab geometry, discretized K_λ^+ functional can be written as:

$$K_\lambda^+[\psi] = K^{+e}[\psi] - \sum_{i=1}^{N_f} I_i[\psi(x_i, \mu)] \tag{3.26}$$

where N_f is the number of interfaces and the interfatial functional I_i is given by

$$I_i[\psi(x_i, \mu)] = \lambda_i^+ \int_{-1}^{+1} \{\mu[\psi(x_{i-}, \mu) - \psi(x_{i+}, \mu)]\} G\{\mu[\psi(x_{i-}, \mu) - \psi(x_{i+}, \mu)]\} d\mu \tag{3.27}$$

Equation (3.27) is the interfacial functional. Substitution of the even parity trial function (3.17) into (3.26) gives the local system of equations for element e and an interfacial system of equations for interface I. The local stiffness matrix obtained in this case is the same as that obtained in case of K^+ principle. The interface matrix A_f^i is obtained by substituting the trial function into the interfacial functional $I_i[\psi(x_i, \mu)]$. The global system of equations is obtained by assembling the local and interfacial systems of equations, which can be represented by:

$$(A + A_f)\underline{\psi} = B \tag{3.28}$$

The global matrix $A + A_f$ obtained in this case is also banded, symmetric and diagonally dominant.

3.5 Determination of Integral Quantities of Interest

After the even parity flux becomes known, the integral quantities of interest can be determined as follows,

- **Element Flux Integral:** This can be determined by integrating over the whole size of the element and over all possible directions,

(3.29)
$$I^e = \int_{x_1^e}^{x_2^e} dx \int_{-1}^{+1} d\mu \phi_0(x,\mu) = \int_{x_1^e}^{x_2^e} dx \int_{-1}^{+1} d\mu \psi_0(x,\mu) = S_1^e \otimes 2\pi \int_{-1}^{+1} Q^{eT}(\mu) d\mu \underline{\psi}^e$$

- **Element Capture Rate:** Once the element flux integral becomes known, element capture rate can be determined by taking its product with the absorption cross-section for that element,

(3.30)
$$C^e = (\sigma^e - \sigma_{s0}^e) I^e$$

- **Element Average Scalar Flux:** This is given by dividing I^e by the size of the element,

(3.31)
$$\overline{\phi^e} = I^e/(x_2^e - x_1^e)$$

- **Element Source Input:** The rate of production of source neutrons in the element (for fixed source problems) is obtained by multiplying the element source strength with the element size,

(3.32)
$$S^e = S(x_2^e - x_1^e)$$

- **Net Element Current:** The net current at a point x in the direction of the x-axis is,

(3.33)
$$J_0(x) = 2\pi \int_{-1}^{+1} \mu G \left[s^- - \mu \frac{\partial \psi_0}{\partial x} \right] d\mu$$

The net current out of an element is then determined by calculating the difference,

(3.34)
$$J_0^e = J_0(x_2^e) - J_0(x_1^e)$$

§4. Numerical results

The comparative study of continuous and discontinuous finite elements is emphasized in this section. The overall computational procedure of the code is shown in the form of a flow diagram in Fig.1. The established K^+ principle for even parity transport equation has been used for the continuous formulation, while the maximum principle K_λ^+ has been utilized for the discontinuous approach.

4.1 A homogeneous slab of a pure absorber

This problem is used by Splawski [13] in a study of the effectiveness of K^+ variational principle for the even parity angular flux. A homogenous slab with thickness $1.0cm$, $\sigma_a = 1.0$, $T_A = 1$, $T_B = 0$ and $S = 0$ is considered. The problem is solved by discretizing the region into 20 linear elements and using different orders of P_N approximations. The results reproduced for scalar flux by using K^+ principle are shown in Fig. (2). The same problem was also run for a discontinuous mesh comprising of 20 linear elements using K^+_λ principle. Therefore, in applying K^+_λ principle, $P_{5,7,9}$ approximation is used in system. Fig. (3) shows the percentage errors in different even parity solutions with respect to the exact solution. As indicated by Figs. (2) and (3) $P_{5,7,9}$ discontinuous solution is in very good agreement with P_9 continuous solution. Comparison of the overall integral quantities obtained in the continuous and discontinuous approaches is given in Table 3.

Table 3: Comparison of Integral Quantities for Homogeneous Slab of a Pure Absorber

Quantity	Exact	K^+ Principle	K^+_λ
Angular Approx.		P_9	$P_{5,9}$
Absorption Rate R	0.3903	0.3925	0.3926
Flux at $x = 0$	1.0	0.9786	0.9796
Flux at $x = 1$	0.1485	0.1477	0.1449
Net Current at $x = 0$	0.5	0.5022	0.5019
Net Current at $x = 1$	0.1097	0.1098	0.1093
Neutron balance	0	4.1828E-05	7.5626E-5

4.2 Repeating lattice cell problems

A thermal nuclear reactor core can be considered to be made up of an assembly of fuel-moderator lattice cells. A schematic diagram for a two region lattice cell problem in slab geometry is illustrated in Fig. (4). The material properties of the fuel and the moderator regions, along with there width are given in Table 4.

Problem 1: A test problem In this problem a unit neutron source is considered in one half $0.0 \leq x \leq 1.0$ of the lattice cell, while a zero source is assumed in the second half $1.0 \leq x \leq 2.0$. The problem is solved with 20 linear elements. P_1, P_3, P_5, P_7, P_9 and a composite $P_{5,9}$ solution for the scalar flux are obtained and compared with the exact solution (see Fig. (5)). K^+_λ principle is used to obtain the $P_{5,9}$ composite solution. The angular flux in this problem is most anisotropic at the point $x = 1.0cm$ because of the change in the source. Therefore, in applying K^+_λ principle a higher order P_9 approximation is used in the region $0.1 \leq x \leq 1.8$ while a lower order P_5 approximation is used for the rest of the system. Fig. (6)

Table 4: Material Properties for Repeating Lattice Cell Problem

Region	Parameter	Problem 1 Test Case	Problem 2 Strong Absorber
Fuel	$\sigma_s(cm^{-1})$	0.37	1.00
	$\sigma_a(cm^{-1})$	0.44	9.00
	Width $a(cm)$	1.00	1.00
Moderator	$\sigma_s(cm^{-1})$	0.37	1.00
	$\sigma_a(cm^{-1})$	0.44	9.00
	Width $a+b(cm)$	2.00	2.00

also shows the percentage errors in different even parity solutions with respect to the exact solution. As indicated by Figs. (5) and (6) $P_{5,9}$ discontinuous solution is in very good agreement with P_9 continuous solution. Table 5 shows the comparison of the integral quantities obtained by both continuous and discontinuous finite elements. This problem was solved exactly by Wilson [14].

Table 5: Comparison of Integral Quantities for Lattice Cell Test Problem

Quantity	K^+ Principle	K^+_λ
Angular Approx.	P_9	$P_{5,9}$
Average Flux	1.1364	1.1364
Capture Rate	1.0	1.0
Source Input	1.0	1.0
Surface Leakage	5.6352E-06	6.0100-09
Neutron balance	5.6352E-06	2.0099-09

Problem 2: A strong absorber lattice cell problem In this problem a medium with large absorption cross section is considered. In the first half of the slab $0.0 \leq x \leq 1.0cm$ a uniform source of neutron is considered which is producing neutrons isotropically at the rate of $10n-cm^{-3}-s-1$. The second half $1.0 \leq x \leq 2.0$ of the slab is strong absorber. A 20 element continuous and discontinuous finite element solutions are compared with the exact solution by Wilson [14] (Fig. (7)). Discontinuous solution is in very good agreement with continuous and exact solutions. The comparison of the integral quantities obtained by both continuous and discontinuous approaches is given in Table 6.

Table 6: Comparison of Integral Quantities for a Strong Absorber Lattice Cell Problem

Quantity	K^+ Principle	K^+_λ
Angular Approx.	P_7	$P_{3,7}$
Average Flux	5.5560E-01	5.5560E-01
Capture Rate	10	10
Source Input	10	10
Surface Leakage	5.0122E-06	2.1675-03
Neutron balance	5.0122E-06	2.1675-03

4.3 Multi-layered shield problem

A multi-layered shield problem with a symmetry about $x = 0$ is considered here. In this problem, there are two layers of fuel materials, two layers of reflecting materials and two layers of thermal and biological shields. The material properties are given in Table 7. The geometry of the problem is shown in Fig. (8). A spatial mesh of 52 linear elements was used for continuous K^+ and discontinuous K^+_λ principles. The scalar flux falls off very rapidly (almost exponentially) in this case as the distance is increased from the center of the core. Use of a P_1 approximation throughout the problem domain gives very poor results, especially near the bare surface boundary. Thus higher order angular approximations were found to be necessary to predict the scalar flux near the bare surface. This problem has been solved exactly for the scalar flux by Galliara [9]. As the order of angular approximation is increased in the continuous formulation, the solution converges (see Fig. (9)). For the discontinuous approach, the angular approximations used in the regions were P_1 , P_3 , and P_7. The composite solution obtained in this manner agrees very well with continuous results (see Fig. 7). The comparison of the integral quantities obtained by both continuous and discontinuous approaches is given in Table 8.

Table 7: Material Properties for Multi-Layered Shield Problem

Region	Total Cross Section $\sigma(cm^{-1})$	Scattering Cross Section $\sigma_s(cm^{-1})$	Source Strength s (arbitray units)
Fuel 1	0.0732	0.0	1.907×10^6
Fuel 2	0.0732	0.0	1.209×10^6
Reflector 1	0.0732	0.0	0.0
Reflector 2	0.0772	0.0	0.0
Iron/Steel	0.1102	0.0	0.0
Concrete	0.07987	0.0	0.0

Table 8: Comparison of Integral Quantities for Multi-layered Shield Problem

Quantity	K^+ Principle	K_λ^+
Angular Approx.	P_7	$P_{1,3,7}$
Average Flux	1.0347E+07	1.0347E+07
Capture Rate	2.7533E+08	2.7533E+08
Source Input	2.7533E+08	2.7533E+08
Surface Leakage	4.0195E-02	4.3187E-02
Neutron balance	6.6362E-02	7.1639E-02

4.4 Reed's edge cell problem

The edge cell problem provides a good test of methods because of different regions have different material properties. Thus in some regions it is necessary to use a high order angular approximation. Suitable composite angular approximations can be chosen for different regions. The edge cell consists of multi-regions with symmetric boundary conditions on the edge only. A four region edge cell with an air-gap is studied using the spatial finite element technique.

This one dimensional slab geometry problem was first studied by Reed [12] using discrete ordinate method. Solution suffered from oscillations in the scalar flux due to the ray effects. Galliara [9] employed K^+ principle to solve this problem using finite elements for spatial variables and Legendre polynomials for angular variables. Smooth results were obtained in this case when mesh refinements were made near material interfaces. These results have been reproduced here in this paper with the computer code which employs the same strategy for continuous approach. The results thus obtained are then compared with the new discontinuous approach implemented using K_λ^+ principle. A discontinuous finite element solution was obtained by Wilson [14] using non-conforming finite elements. He used K^{+-} variational principle, which employs both even and odd-parity fluxes. In the present scheme only even-parity flux is being used, thus reducing the number of unknowns by at least one half as compared to K^{+-} principle.

The geometry of the problem is shown in Fig. (10). The cell is made up of five regions, material properties of which are given in Table 9. The edge cell problem provides a strenuous test for the numerical approximation methods due to presence of strong heterogeneities in the material properties of various regions in the cell over very small distances. A spatial mesh of 58 linear elements was used for continuous K^+ and discontinuous K_λ^+ principles (see Fig. (11)). Higher order angular approximations were used in regions where the transport effects are more prominent, while lower order approximations were found to be sufficient in the remaining regions. A P_3 approximation is chosen in region 5 where the angular flux is fairly anisotropic. The angular flux in regions 2 and 4 is highly anisotropic and therefore also highly anisotropic in region 3 (the air gap). Therefore, P_7 approximation is adopted in these

regions. A P_1 approximation with only two elements in $0.0 \leq x \leq 1.9$ region of the fuel material was found to be sufficient to estimate the correct scalar flux. The scalar flux of this problem was calculated using F_N method by Garcia and Siewert [10]. The comparison of the integral quantities by both continuous and discontinuous approaches is given in Table 10.

Table 9: Material Properties for Edge Cell Problem

Region	Total Cross Section $\sigma(cm^{-1})$	Scattering Cross Section $\sigma_s(cm^{-1})$	Source Strength s (arbitray units)
Fuel	50.0	0.0	50.0
Clad	5.0	0.0	0.0
Air gap	1×10^{-3}	0.0	0.0
Moderator 1	1.0	0.9	1.0
Moderator 2	1.0	0.9	0.0

Table 10: Comparison of Integral Quantities for Edge Cell Problem

Quantity	K^+ Principle	K^+_λ
Angular Approx.	P_7	$P_{1,3,7}$
Average Flux	9.5360E-01	9.5620E-01
Capture Rate	1.0087E+02	1.0087E+02
Source Input	1.0100E+02	1.0100E+02
Surface Leakage	1.3150E-01	1.3157E-01
Neutron balance	1.6408E-04	1.7499E-04

§5. Conclusions

In this paper a variational formulation of the even parity transport equation has been presented for solving neutron transport problems using discontinuous finite elements approach. Numerical simulations have been carried out in Matlab®to test the variational scheme. Both continuous and discontinuous finite element options have been implemented to solve one dimensional slab geometry, one group fixed source problems. The spatial dependence of the even-party angular flux has been modeled using finite elements and directional dependence has been expanded in terms of even Legendre moments. Composite solutions were obtained by varying the order of angular approximations in different parts of the system. It was found that a P_1 approximation could be employed in regions where the angular flux was almost isotropic and give an accurate solution. A high order P_N approximation is adopted in regions of highly anisotropic angular flux. Several one group slab geometry problems were solved nu-

merically. Results were found to be in excellent agreement with analytical results as well as with conventional continuous finite element method results.

Acknowledgements: This work has been sponsored by the Higher Education Commission, Government of Pakistan under the scholarship grants No. 17-6(174)/Sch/2001. Study leave grant of second author (Mr. Shaukat Iqbal) from Pakistan Atomic Energy Commission is also highly appreciated.

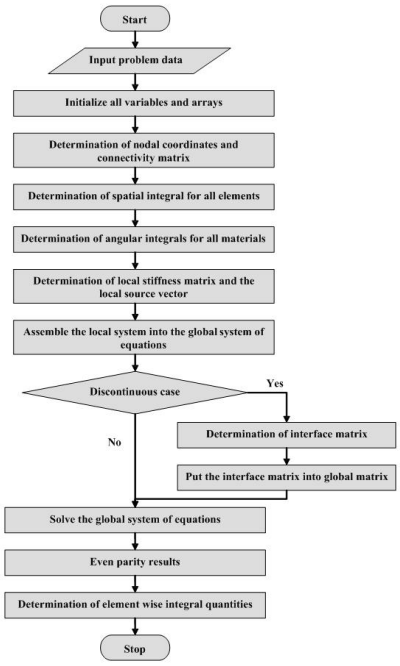

Figure 1: Flow chart of the code for even-parity Boltzmann transport equation

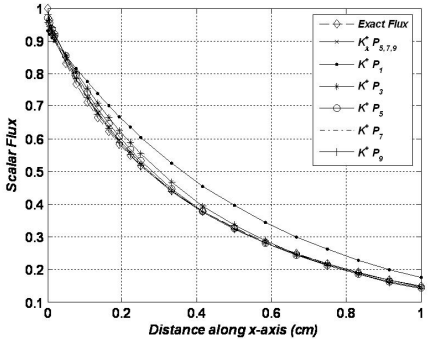

Figure 2: Even parity solutions (scalar flux) using K^+ and K^+_λ principles for homogenous slab of pure absorber

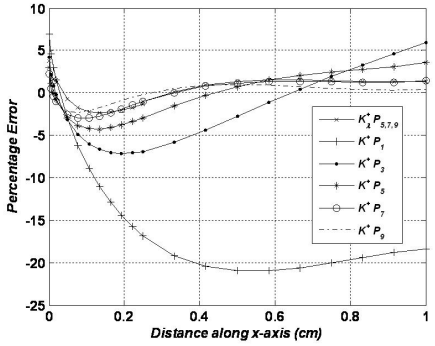

Figure 3: Percentage error for homogenous slab of pure absorber with respect to exact solution

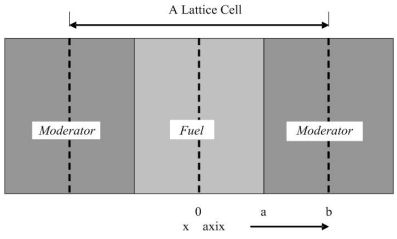

Figure 4: Geometry of two region lattice cell problem

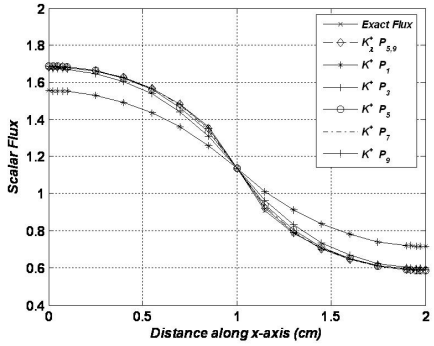

Figure 5: Even parity solutions (scalar flux) using K^+ and K_λ^+ principles for lattice cell test problem

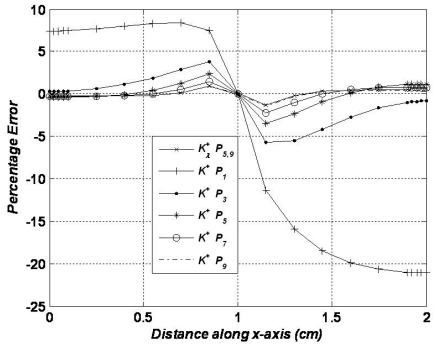

Figure 6: Percentage errors for lattice cell test problem with respect to the exact solution

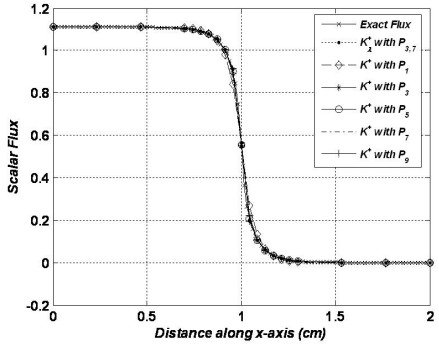

Figure 7: Scalar flux using K^+ and K^+_λ principles for strong absorber lattice cell problem

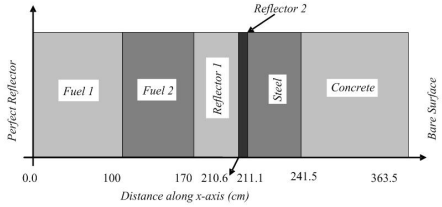

Figure 8: Geometry of for multi-layered shield problem

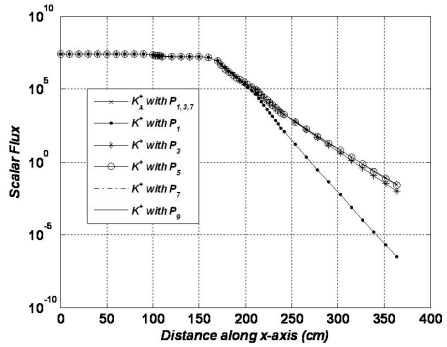

Figure 9: Even parity solutions (scalar flux) using K^+ and K^+_λ principles for multi-layered shield problem

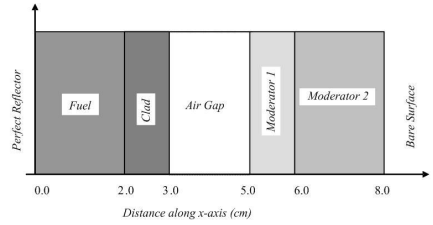

Figure 10: Geometry of for edge cell problemn

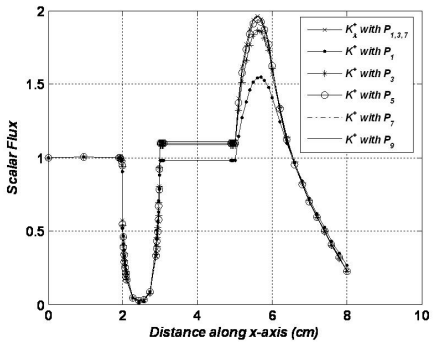

Figure 11: Even parity solutions (scalar flux) using K^+ and K_λ^+ principles for edge cell problem

References

[1] R.T. Ackroyd, *A finite element method for Neutron transport - VII. Completely boundary free maximum principles for the first-order Boltzmann equation*, Annal of Nulcear Energy 10 (1983), 243-261.

[2] R.T. Ackroyd, *Finite element method for Neutron transport based on maximum and minimum principles for discontinuous trial functions*, Ann. Nucl. Energy 19 (1992), 565-592.

[3] R.T. Ackroyd, *Generalized least squares as a generator of variational principles and weighted residual methods for FEM transport problems*, Progress in Nuclear Energy 18, 1/2 (1986), 45-62.

[4] R.T. Ackroyd, O.A. Abuzid, A.M. Mirza, *Discontinuous finite element solutions for Neutron transport in X-Y geometry*, Ann. Nucl. Energy 22 (1995), 181-201.

[5] R.T. Ackroyd and W.E. Wilson, *Composite finite element solutions for Neutron transport*, Annals of Nuclear Energy 15 (1988), 397-419.

[6] J.A. Davis, *Transport error bounds via PN approximation*, Nucl. Sci. & Eng. 31 (1968), 166-176.

[7] C.R.E. De Oliveira, *Finite Element Technique for Multigroup Neutron Transport Calculations with Anisotropic Scattering*, PhD Thesis, University of London, 1987.

[8] J. Duderstadt and R.M.William, *Transport Theory*, John Wiley & Sons, 1979.

[9] J. Galliara and M.M.R. Williams, *A finite element method for Neutron transport - II, some practical considerations*, Ann. Nucl. Energy 6 (1979), 205-223.

[10] R.D.M. Garcia and C.E. Siewert, *A multigroup calculation in the Theory of Neutron diffusion*, Nucl. Sci. & Eng. 76 (1980), 53-56.

[11] A.M. Mirza, *Discontinuous Finite Element Formulation of the Neutron Transport Equation*, PhD Thesis, University of London, 1995.

[12] W.H. Reed, *New difference schemes for the Neutron transport equation*, Nucl. Sci. & Eng. 46 (1971), 309-319.

[13] B.A. Splawski, *Finite Element Method for Neutron Transport Calculations*, PhD Thesis, University of London, 1981.

[14] W.E. Wilson, *Discontinuous Finite Elements for Neutron Transport Analysis*, PhD Thesis, University of London, 1985.

Authors' addresses:

Anwar M. Mirza and Shaukat Iqbal
Faculty of Computer Science and Engineering,
Ghulam Ishaq Khan (GIK) Institute of Engineering Sciences and Technology,
Topi, 23460, Swabi, PAKISTAN
e-mail: anwar.m.mirza@gmail.com, shaukat@giki.edu.pk

First author's current address:
Department of Computer Science,
National University of Computer and Emerging Sciences (FAST-NU),
A.K. Brohi Road, Sector H-11, Islamabad, PAKISTAN
email: anwar.m.mirza@nu.edu.pk